Analysis of air-launched ground-penetrating radar techniques to measure the soil surface water content

Sébastien Lambot,[1,2] Lutz Weihermüller,[1] Johan A. Huisman,[1] Harry Vereecken,[1] Marnik Vanclooster,[2] and Evert C. Slob[3]

Received 12 April 2006; revised 6 July 2006; accepted 24 July 2006; published 3 November 2006.

[1] We analyze the common surface reflection and full-wave inversion methods to retrieve the soil surface dielectric permittivity and correlated water content from air-launched ground-penetrating radar (GPR) measurements. In the full-wave approach, antenna effects are filtered out from the raw radar data in the frequency domain, and full-wave inversion is performed in the time domain, on a time window focused on the surface reflection. Synthetic experiments are performed to investigate the most critical hypotheses on which both techniques rely, namely, the negligible effects of the soil electric conductivity (σ) and layering. In the frequency range 1–2 GHz we show that for $\sigma > 0.1$ Sm^{-1}, significant errors are made on the estimated parameters, e.g., an absolute error of 0.10 in water content may be observed for $\sigma = 1$ Sm^{-1}. This threshold is more stringent with decreasing frequency. Contrasting surface layering may proportionally lead to significant errors when the thickness of the surface layer is close to one fourth the wavelength in the medium, which corresponds to the depth resolution. Absolute errors may be >0.10 in water content for large contrasts. Yet we show that full-wave inversion presents valuable advantages compared to the common surface reflection method. First, filtering antenna effects may prevent absolute errors >0.04 in water content, depending of the antenna height. Second, the critical reference measurements above a perfect electric conductor (PEC) are not required, and the height of the antenna does not need to be known a priori. This averts absolute errors of 0.02–0.09 in water content when antenna height differences of 1–5 cm occur between the soil and the PEC. A laboratory experiment is finally presented to analyze the stability of the estimates with respect to actual measurement and modeling errors. While the conditions were particularly well suited for applying the common reflection method, better results were obtained using full-wave inversion.

Citation: Lambot, S., L. Weihermüller, J. A. Huisman, H. Vereecken, M. Vanclooster, and E. C. Slob (2006), Analysis of air-launched ground-penetrating radar techniques to measure the soil surface water content, *Water Resour. Res.*, *42*, W11403, doi:10.1029/2006WR005097.

1. Introduction

[2] Knowledge of the spatial distribution and dynamics of the surface water content at various scales is essential in agricultural, hydrological, meteorological, and climatological research and applications. Surface water content constitutes the boundary condition between the soil and the atmosphere and governs all important key processes such as infiltration, runoff, evaporation, as well as partitioning of energy at the Earth's surface into sensible and latent exchange with the atmosphere. In catchment hydrology, for instance, the readiness of an area to generate surface runoff during storm rainfall is related to its surface storage capacity, a variable which can be computed accurately when surface water content is known. Disregarding the spatial variability of the surface water content may contribute significantly to errors on surface runoff estimation, even at a limited spatial scale [e.g., *Merz and Bardossy*, 1998].

[3] Existing techniques to characterize soil surface water content are either suited to small areal scales (<0.1 m), such as the gravimetric method, capacitive sensors, and time domain reflectometry (TDR), or to large areal scales (>10–100 m), such as airborne and spaceborne passive microwave radiometry and active radar systems [e.g., *Dobson and Ulaby*, 1986; *Jackson et al.*, 1996; *Huisman et al.*, 2002]. As yet, no practical method is available to measure the variability of soil surface water content at field or watershed scales, which is crucial in applications that include agricultural water management and soil and water conservation, among others, and to bridge the scale gap between airborne and spaceborne remote sensing and ground truth measurements [*Famiglietti et al.*, 1999]. In

[1] Agrosphere (ICG IV), Institute of Chemistry and Dynamics of the Geosphere, Forschungszentrum Jülich GmbH, Jülich, Germany.
[2] Department of Environmental Sciences and Land Use Planning, Université catholique de Louvain, Louvain-la-Neuve, Belgium.
[3] Department of Geotechnology, Delft University of Technology, Delft, Netherlands.

0043-1397/06/2006WR005097

that respect, ground-penetrating radar (GPR) is a very promising tool for mapping the soil surface properties at an intermediate scale (0.1–100 m) and is currently the subject of active research with respect to soil water measurement. A review of GPR principles and history is given by *Annan* [2002] and reviews on its application for measuring soil water content are given by *Davis and Annan* [2002] and *Huisman et al.* [2003].

[4] For identifying surface water content, two GPR approaches are commonly used. First, the surface water content can be derived from the ground wave propagation velocity [*Du and Rummel*, 1994; *Huisman et al.*, 2001, 2002; *Galagedara et al.*, 2003; *Grote et al.*, 2003; *Galagedara et al.*, 2005a, 2005b]. The limitations of the technique for practical field applications are the required contact between the antennas and the soil, the identification of the ground wave, which may be ambiguous or even impossible in some conditions, and the presence of ambiguous guided waves when near-surface layering is present. The second approach is the surface reflection coefficient method, which uses air-launched radar configurations [*Chanzy et al.*, 1996; *Redman et al.*, 2002; *Serbin and Or*, 2003, 2004]. Notwithstanding the practical appropriateness of this method for mapping applications, the method still remains largely unexplored nowadays. The concept is however commonly used in airborne and spaceborne radar remote sensing for the retrieval of soil surface water content [e.g., *Ulaby et al.*, 1986].

[5] Recently, *Lambot et al.* [2004c] proposed a new promising approach for identifying the soil hydrogeophysical properties using GPR. Relying on an adequate electromagnetic model describing the radar-antenna-subsurface system, the method is based on full-wave inversion of the GPR signal in the frequency domain for an off-ground monostatic antenna configuration. In contrast to other existing GPR characterization techniques, this method accounts for the major antenna effects and includes spherical divergence in wave propagation. Moreover, all the information contained in the radar signal is used in the inversion process. The method has been successfully used in a series of well-controlled laboratory applications [*Lambot et al.*, 2004b, 2004a, 2005a]. *Lambot et al.* [2005b] have adapted the method to the identification of the surface dielectric permittivity and correlated water content for uncontrolled field conditions. For that purpose, inversion is performed in the time domain and is focused on the surface reflection only.

[6] In this paper, we analyze the main hypotheses on which the proposed full-wave inversion approach relies for the identification of the surface water content and we compare the technique to the common surface reflection method, thereby extending the work of *Lambot et al.* [2005b]. In particular, we investigate the effect of the electric conductivity and near-surface layering on the retrieval of the surface water content using numerical experiments. Two different operating frequency ranges and different moisture conditions are considered. Finally, laboratory experiments are performed to examine the effect of realistic modeling and measurements errors on the estimated parameters, i.e., to examine the stability of the inverse solution.

[7] An additional hypothesis, which may be critical to the applicability of the method in real field conditions, is the smoothness of the soil surface, whereas roughness and vegetation are generally present in the real world. However, as shown by *Lambot et al.* [2006], the effect of surface heterogeneity on the full-wave inversion of off-ground radar data may be negligible provided that the operating wavelength is sufficiently large compared to the heterogeneity amplitude. In particular, at least Rayleigh's criterion should be respected [e.g., see *Ulaby et al.*, 1986; *Boithias*, 1987]. In that case, for instance, a roughness amplitude of about 10 cm would require radar frequencies lower than 375 MHz so that the soil appears smooth. In case the spatial resolution requirements do not permit to lower the operating frequency band, it is necessary to include surface heterogeneity in the radar wave propagation model [e.g., see *Warnick and Chew*, 2001]. The presence of plants may also affect to some extent the radar measurements, depending on biomass density and distribution [*Serbin and Or*, 2005].

2. Theory

2.1. Common Surface Reflection Method

[8] The common surface reflection method applies to air-launched GPR configurations, either monostatic or bistatic, and is based on the determination of the reflection coefficient of the soil surface interface. The following assumptions are particularly considered: (1) the antennas are located in free space (air) above a homogeneous half-space (soil) limited by a plane interface, (2) the reflection coefficient can be approximated by the plane wave reflection coefficient, (3) antenna distortion effects are negligible, (4) the soil electric conductivity is assumed to be negligible, (5) the magnetic permeability is assumed to be equal to the free space permeability, and (6) the dielectric permittivity is frequency-independent.

[9] As a result, the reflection coefficient at the soil interface is a Dirac's delta function of time and its amplitude is defined as the ratio between the backscattered (E_s) and incident (E_i) electric fields. For a normal incidence plane wave, the amplitude R of the reflection coefficient can thus be expressed as:

$$R = \frac{1 - \sqrt{\varepsilon_r}}{1 + \sqrt{\varepsilon_r}} \tag{1}$$

where ε_r is the relative dielectric permittivity of the soil. The soil dielectric permittivity can therefore be derived as:

$$\varepsilon_r = \left(\frac{1 - R}{1 + R}\right)^2 \tag{2}$$

The reflection coefficient R is usually determined from the measured amplitude of the soil surface reflection, A, relative to the amplitude measured for a perfect electric conductor (PEC) situated at the same distance as the soil, namely, A_{PEC}. The ratio between the reflection coefficient at the soil surface interface (R) and at a PEC interface (R_{PEC}) can be expressed as:

$$\frac{R}{R_{PEC}} = \frac{\frac{E_s}{E_i}}{\frac{E_{s,PEC}}{E_i}} \tag{3}$$

Since $R_{PEC} = -1$, assuming E_i to be constant, and assuming that the measured amplitude A is directly proportional to the

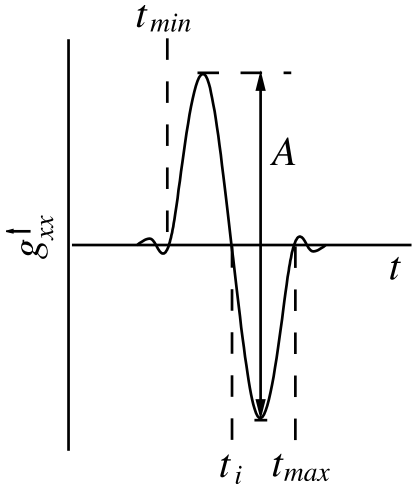

Figure 1. Sketch of the radar signal in the time domain, $g^{\uparrow}_{xx}(t)$, from which antenna effects have been filtered out. Times $t_{\min}$ and $t_{\max}$ define the time window focused on the surface reflection in which inversion is performed; t_i is the time corresponding approximately to the surface interface in the space domain. A is the amplitude of the reflection considered when using the common surface reflection method, although the surface reflection has a different shape as it contains partly antenna effects.

backscattered electric field E_s, i.e., there are no antenna distortion effects, (3) reduces to:

$$R = -\frac{E_s}{E_{s,PEC}} = -\frac{A}{A_{PEC}} \tag{4}$$

In this paper, a stepped frequency continuous wave (SFCW) radar is used and measurements are performed over a limited frequency range with a constant amplitude sweep. In this case, the amplitude A is defined as the difference between the maximum and minimum peaks of the surface reflection, as illustrated in Figure 1. Figure 1 is discussed below.

2.2. Full-Wave Inversion Method

[10] The SFCW radar system we use consists of a vector network analyzer (VNA) connected to an ultrawide band monostatic horn antenna used off the ground. For this specific configuration, the following frequency domain radar equation holds [*Lambot et al.*, 2004c]:

$$S_{11}(\omega) = H_i(\omega) + \frac{H(\omega)G^{\uparrow}_{xx}(\omega)}{1 - H_f(\omega)G^{\uparrow}_{xx}(\omega)} \tag{5}$$

where S_{11} is the quantity measured by the VNA, H_i is the antenna return loss, H is the antenna transmitting-receiving transfer function, H_f is the antenna feedback loss, $G^{\uparrow}_{xx}$ is the transfer Green's function of the air and subsurface, and ω is the angular frequency. The Green's function represents the solution of the three-dimensional (3-D) Maxwell's equations for electromagnetic waves propagating in multilayered media [e.g., *Michalski and Mosig*, 1997]. The consideration of a 3-D model is essential to take into account spherical divergence (geometric spreading) in wave propagation. This radar equation permits to filter out the major antenna effects from the measured radar signal $S_{11}(\omega)$. The reader is referred to *Lambot et al.* [2004c, 2006] for additional details on this model and the determination of the antenna transfer functions.

[11] In order to identify the surface dielectric permittivity and correlated water content, we focus full-wave inversion of the Green's function in the time domain on the surface reflection [*Lambot et al.*, 2005b]. The measured and modeled frequency domain Green's functions are first transformed in the time domain using the inverse Fourier transform:

$$g^{\uparrow}_{xx}(t) = \mathrm{F}^{-1}\left\{G^{\uparrow}_{xx}(\omega)\right\} = \frac{1}{2\pi}\int_{-\infty}^{\infty} e^{i\omega t}G^{\uparrow}_{xx}(\omega)d\omega \tag{6}$$

where ω is the angular frequency, t is time, and $i = \sqrt{-1}$. Then, a time window is defined between $t_{\min}$ and $t_{\max}$, focused on the surface reflection (see Figure 1). It is worth noting that since measurements are performed over a limited frequency range with a constant amplitude sweep, the surface reflection in $g^{\uparrow}_{xx}(t)$ tends to be antisymmetric (see also Figure 1). The root t_i of the signal between the positive and negative peaks of the reflection corresponds exactly to the surface interface in the space domain only under the hypotheses of the common surface reflection method. In practice, t_i does not correspond precisely to the surface interface because the reflection coefficient is time-dependent because of (1) geometrical spreading in wave propagation (the reflection originates mainly from the Fresnel zone), (2) the delaying effect of electric conductivity, and (3) the distortion effects due to the frequency dependence of the soil electromagnetic properties.

[12] The inverse problem is formulated in the least squares sense and the objective function is accordingly defined as follows:

$$\phi(\mathbf{b}) = \left(\mathbf{g}^{\uparrow *}_{\mathbf{xx}} - \mathbf{g}^{\uparrow}_{\mathbf{xx}}\right)^T\left(\mathbf{g}^{\uparrow *}_{\mathbf{xx}} - \mathbf{g}^{\uparrow}_{\mathbf{xx}}\right) \tag{7}$$

where

$$\mathbf{g}^{\uparrow *}_{\mathbf{xx}} = g^{\uparrow *}_{xx}(t)|^{t_{\max}}_{t_{\min}} \quad \text{and} \quad \mathbf{g}^{\uparrow}_{\mathbf{xx}} = g^{\uparrow}_{xx}(t)|^{t_{\max}}_{t_{\min}} \tag{8}$$

are the vectors containing, respectively, the observed and simulated time domain windowed Green's functions, and $\mathbf{b} = [\varepsilon_{r,1}, d_0]$ is the parameter vector to be estimated with $\varepsilon_{r,1}$ being the soil surface relative dielectric permittivity and d_0 being the distance between the antenna phase center and the soil surface interface. Subscripts 0 and 1 denote, respectively, the air and first soil layers. As for the common surface reflection method, the electric conductivity, magnetic permeability, and soil layering are assumed to have a negligible effect on the estimation of $\varepsilon_{r,1}$. The model configuration used for the inversion consists thus of a point source above a 3-D lower half-space, as sketched in Figure 2a.

[13] The 2-D objective function (7) is minimized using the local Nelder-Mead simplex algorithm [*Lagarias et al.*, 1998]. An initial guess for the antenna elevation d_0 is derived from the root t_i of the signal between the positive and negative peaks of the surface reflection (see Figure 1). The initial guess for the relative dielectric permittivity is arbitrary chosen in the range $2.5 \leq \varepsilon_r \leq 20$. We have

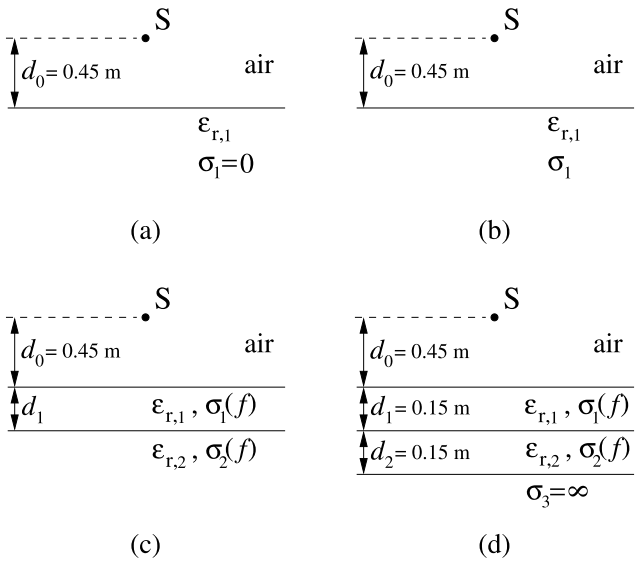

Figure 2. Model configurations for the numerical experiments. S is the point source and receiver corresponding to the antenna phase center. (a) Source above a lossless dielectric half-space. This configuration is used for the inversions. (b) Source above a lossy dielectric half-space. (c) Source above a two-layered medium with varying layer thicknesses d_1 and assuming the apparent electric conductivity to be frequency dependent. (d) Configuration corresponding to the laboratory experiment.

verified that this procedure leads always to the global minimum of the objective function (results not shown).

3. Numerical Experiments

3.1. Model Configurations

[14] The objective of the numerical experiments is to investigate the most critical hypotheses under which the estimation procedures described above apply. Namely, we analyze the effects of the electric conductivity and near-surface layering on the inverse retrieval of the surface water content. These two factors are neglected in both the common reflection and inversion methods. The analysis is performed for two different GPR frequency ranges, namely, 100–900 MHz and 1000–2000 MHz. Figure 2 represents the four model configurations for which synthetic Green's functions were generated.

[15] Configuration a corresponds to the basic model which is used for the inversion. It consists of only a half-space whose electric conductivity σ_1 is equal to zero and whose dielectric permittivity $\varepsilon_{r,1}$ takes nine different values, corresponding realistically to the nine volumetric water contents (θ) of a sand as described by *Lambot et al.* [2004c] (θ = 0.010, 0.035, 0.072, 0.111, 0.158, 0.195, 0.218, 0.252, 0.263). The relation between the dielectric permittivity and the volumetric water content is described by the model of *Ledieu et al.* [1986]:

$$\theta = a\sqrt{\varepsilon_r} + b \tag{9}$$

with a = 0.1264 and b = −0.1933 being sand specific parameters. Configuration b includes the electric conductivity, corresponding as well to actual values for the nine water contents above. The considered electric conductivity is a frequency averaged apparent electric conductivity, i.e., including dielectric losses. Configuration c includes an additional layer with five different thicknesses (d_1 = 0.005, 0.01, 0.02, 0.04, 0.08 m), that is subject to a single water content (θ = 0.158). The lower half-space is subject to the nine water contents above. The frequency dependence of the apparent electric conductivity is taken into account. Configuration d sketches the laboratory experiment presented below, where the top layer is subject to the nine water contents, the second layer only to one (θ = 0.100), and the lower half-space emulates a PEC ($\sigma = \infty$), thereby constituting a perfect reflector. In total, 144 synthetic Green's functions were generated for these four model configurations (9 water contents ×(3 + 5) model structures ×2 frequency ranges).

[16] For comparison purposes, the retrieval of the surface dielectric permittivity from the synthetic data has also been done using the common surface reflection method. Since with this method it is assumed that the measurements above the soil are taken at the same distance d_0 as the corresponding measurements above the PEC, which is inherently never exactly true in practical applications, we considered three cases: (1) an antenna elevation error Δd_0 = 0 cm, (2) Δd_0 = 1 cm, and (3) Δd_0 = 5 cm. Moreover, in common GPR approaches the Green's function of the air-soil system is unknown because no appropriate radar model permits to compute it from the raw radar data, which include all antenna effects. Hence we extracted the reflection coefficient R from the reconstructed radar signal using (5). We used the transfer functions of the antenna utilized for the laboratory experiment presented below. Yet, H_i being usually removed from the signal in this radar mode of operation, as it can be readily measured by performing a free space measurement [e.g., *Serbin and Or*, 2004], we computed the reflection coefficient from the synthetic $S_{11}^*(\omega) = S_{11}(\omega) - H_i(\omega)$, that includes partly antenna distortion effects ($H(\omega)$ and $H_f(\omega)$). In a bistatic mode of operation, H_i would correspond to the direct coupling between the emitting and receiving antennas.

[17] It is worth noting that for $s_{11}^*(t)$ in the time domain, time zero does not correspond to the antenna phase center but to the VNA calibration plane, i.e., to the connection between the cable and the antenna. For common time domain radar systems, time zero is usually not well defined [*Yelf*, 2004]. For $G_{xx}^{\uparrow}$, time zero corresponds to the antenna phase center from which apparent spherical divergence is initiated.

3.2. Standard Error of the Estimated Parameters

[18] Table 1 shows the numerical results for configurations a, b, and d. Results are expressed in terms of the standard error s on the estimated relative dielectric permittivity and corresponding volumetric water content, averaged with respect to the nine water contents:

$$s_{\varepsilon_r} = \left(\frac{1}{N-1} \sum_{n=1}^{N} \left[\left(\varepsilon_{r,n}^* - \varepsilon_{r,n} \right) - \overline{\left(\varepsilon_r^* - \varepsilon_r \right)} \right]^2 \right)^{\frac{1}{2}} \tag{10}$$

$$s_\theta = \left(\frac{1}{N-1} \sum_{n=1}^{N} \left[\left(\theta_n^* - \theta_n \right) - \overline{\left(\theta^* - \theta \right)} \right]^2 \right)^{\frac{1}{2}} \tag{11}$$

Table 1. Standard Error on the Estimated Relative Dielectric Permittivity ε_r and Corresponding Water Content θ for the Different Experiments[a]

	Standard Error s			
	100–900 MHz		1000–2000 MHz	
	$s_{\varepsilon r,1}$	$s_{\theta 1}$	$s_{\varepsilon r,1}$	$s_{\theta 1}$
Model Configuration a: Source Over a Lossless Dielectric Half-Space				
Inversion method	3.22e-5	8.53e-7	2.72e-5	6.94e-7
Common reflection method (Δd_0 = 0 cm)	9.70e-2	1.24e-3	1.55e-2	2.09e-4
Common reflection method (Δd_0 = 1 cm)	1.64e-1	2.96e-3	3.56e-1	5.62e-3
Common reflection method (Δd_0 = 5 cm)	1.59e-0	2.41e-2	1.90e-0	2.80e-2
Model Configuration b: Source Over a Conductive Dielectric Half-Space				
Inversion method	2.67e-1	4.95e-3	3.79e-2	7.12e-4
Common reflection method (Δd_0 = 0 cm)	1.01e-1	1.91e-3	1.53e-2	2.53e-4
Common reflection method (Δd_0 = 1 cm)	2.49e-1	4.51e-3	3.60e-1	5.72e-3
Common reflection method (Δd_0 = 5 cm)	1.69e-0	2.57e-2	1.91e-0	2.81e-2
Model Configuration d: Three-Layered Laboratory Setup				
Inversion method	2.96e-1	7.01e-3	2.47e-1	5.68e-3
Common reflection method (Δd_0 = 0 cm)	4.66e-1	1.63e-2	3.48e-1	1.01e-2
Common reflection method (Δd_0 = 1 cm)	5.19e-1	1.63e-2	5.46e-1	1.10e-2
Common reflection method (Δd_0 = 5 cm)	1.78e-0	2.85e-2	2.06e-0	2.90e-2
Laboratory Experiment				
Reference method	–	–	3.35e-1	8.23e-3
Inversion method	–	–	1.07e-0	2.22e-2
Common reflection method	–	–	1.19e-0	2.81e-2

[a]Results are presented for the inversion and common surface reflection methods. Different errors Δd_0 on the antenna elevation above the ground are considered. Read 3.22e-5 as 3.22×10^{-5}.

where $N = 9$ is the total number of water contents, n refers to a specific water content, ε_r^* and ε_r are the estimated and actual relative dielectric permittivities and θ^* and θ are the estimated and actual volumetric water contents, respectively. Results for configuration c are not presented in Table 1 because the standard error depends strongly on the water content and is therefore not normally distributed (see below).

3.2.1. Model Configuration a: Source Over a Lossless Dielectric Half-Space

[19] For configuration a, where we have the source and receiver situated above a nonconductive dielectric half-space (see Figure 2a), errors are negligible for both frequency ranges, demonstrating the uniqueness of the inverse solution, i.e., enough information is contained in the radar signal to retrieve the surface dielectric permittivity from the surface reflection only. The common reflection method appears to be less accurate than the full-wave inversion method (frequency averaged standard error on θ: $s_{\theta 1} = 7.25 \times 10^{-4}$ compared to about 7.74×10^{-7} for the inversion). In particular, an error on the antenna elevation Δd_0 can result in a significant error on the estimated dielectric permittivity and calculated water content ($s_{\theta 1} = 4.29 \times 10^{-3}$ for $\Delta d_0 = 1$ cm and $s_{\theta 1} = 2.61 \times 10^{-2}$ for $\Delta d_0 = 5$ cm). This substantial issue is not encountered with the full-wave inversion method.

[20] When no error in the antenna elevation is assumed ($\Delta d_0 = 0$), the remaining error with the common surface reflection method stems from the antenna dispersive effects. Figure 3 represents the radar signals $s_{11}^*(t)$ (including antenna effects H and H_f) and $g_{xx}^{\uparrow}(t)$ (free of antenna effects)

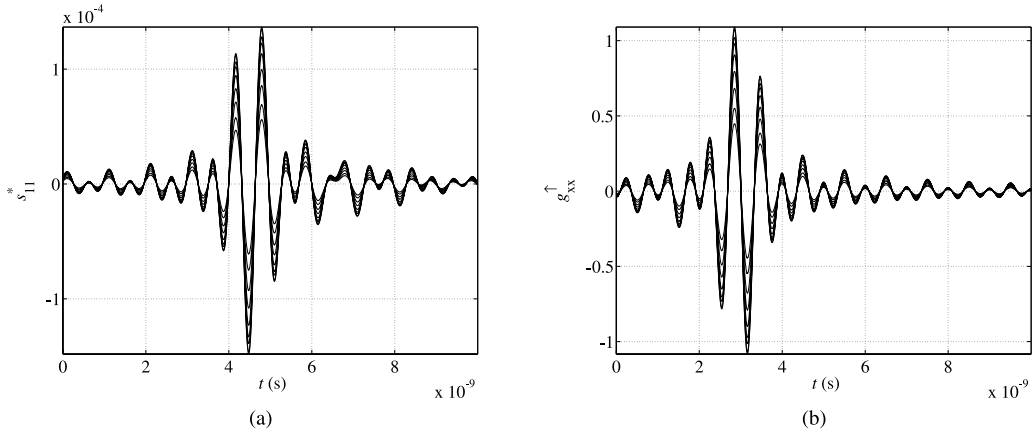

Figure 3. (a) The s_{11}^* (raw radar data $-H_i$) and (b) $g_{xx}^{\uparrow}$ (antenna effects are completely filtered) for a source over a lossless dielectric half-space and the nine water contents.

for the nine water contents. We can clearly see how the radar signal is affected by the antenna, i.e., $s_{11}^{*}(t)$ is significantly different from $g_{xx}^{\uparrow}(t)$. In particular, the time at which the surface reflection occurs in $s_{11}{}^{*}(t)$ is ambiguous, complicating the correct estimation of the antenna elevation from the reflection. The antisymmetric shape of the surface reflection is not preserved in $s_{11}{}^{*}(t)$, making difficult to identify which part of the signal in the time domain corresponds to the surface interface in the space domain. In addition, time $t = 0$ does not correspond anymore to the antenna phase center and is therefore also ambiguous because it includes the two-way antenna propagation time. In practical applications of the common reflection method, the antenna elevation should therefore be determined independently.

[21] We have performed the same analysis for an antenna elevation d_0 = 15 cm in the frequency range 1000–2000 MHz, with $\Delta d_0 = 0$. We obtained $s_{\theta 1} = 5.69 \times 10^{-7}$ for the inversion method and $s_{\theta 1} = 1.29 \times 10^{-2}$ for the common surface reflection method. In this case antenna effects lead to significant errors on the estimation of the soil surface water content. This detrimental effect results from the increasing interferences between the surface reflection and the multiple internal antenna reflections when the antenna approaches the soil. This issue should also be taken into account when using the common surface reflection method.

[22] The inverse estimation of the antenna elevation, d_0, is very accurate for the inversion method. The average error performed on the inverse estimation of d_0 is -2.37×10^{-8} m and is to be attributed to numerical artifacts. When deriving d_0 from t_i, the average error is 7.54×10^{-4} m. As explained above, this larger error originates from the time dependence of the reflection coefficient. However, for this particular case, the error remains negligible.

3.2.2. Model Configuration b: Source Over a Conductive Dielectric Half-Space

[23] In configuration b, the source is situated above a conductive dielectric half-space (see Figure 2b). Inversion results for that model show that less satisfactory estimates are obtained when the soil is lossy. This detrimental effect is one order of magnitude larger in the low-frequency range than in the high frequency range. This is due to the fact that the imaginary part of the propagation wave number containing the effect of the electric conductivity is divided by the angular frequency. We observe that the inversion method leads to slightly less accurate results compared to the common reflection method when $\Delta d_0 = 0$. This may be attributed to the fact that for the inversion method, d_0 is an additional unknown and some correlation different from 0 may exist between d_0 and $\varepsilon_{r,1}$ in the inversion process. Results in favor of the inversion method would have been obtained for smaller distances d_0 between the antenna and the soil, as shown in previous section.

[24] Figures 4 and 5 represent, respectively, the 100–900 MHz and 1000–2000 MHz response surfaces of the objective function in the $\varepsilon_{r,1} - d_0$ and $\varepsilon_{r,1} - \sigma_1$ parameter planes for three different water contents. The range of each parameter has been divided into 100 discrete values resulting in 10000 objective function calculations for each contour plot. First, we observe as expected that the solution, i.e., the minimum of the objective function, is unique in the $\varepsilon_{r,1} - d_0$ parameter plane. This parameter pair is not correlated, but the sensitivity of the objective function with respect to $\varepsilon_{r,1}$ decreases when $\varepsilon_{r,1}$ increases. In other words, the uncertainty on $\varepsilon_{r,1}$ increases when this parameter increases. The topography of the objective function is quite simple, which is advantageous for a rapid and robust optimization. Because of $\sigma_1 \neq 0$, the minimum of the objective function does not correspond exactly to the true parameter values. Assuming $\sigma_1 = 0$ introduces therefore an error on the estimated parameters, but this error appears to be negligible (see below).

[25] In the $\varepsilon_{r,1} - \sigma_1$ parameter plane, we observe a poor sensitivity of the objective function with respect to σ_1 if σ_1 is sufficiently low. The commonly used assumption of a negligible electric conductivity when considering the surface reflection relies on this low sensitivity. In the range 100–900 MHz, σ_1 should be ideally $<\sim 10^{-2}$ Sm^{-1} and in the range 1000–2000 MHz σ_1 should be ideally $<\sim 10^{-1}$ Sm^{-1}. In the environment, these conditions may not be satisfied in wet soils or soils with a high clay content. For both frequency ranges, neglecting σ_1 when $\sigma_1 > 10^{-1}$ Sm^{-1} would lead to unrealistic values for $\varepsilon_{r,1}$, and hence also for the estimation of the correlated water content. *al Hagrey and Müller* [2000] also observed that $\sigma > 0.1$ Sm^{-1} may have a significant impact on the surface reflection coefficient. It is worth noting that the electric conductivity we speak about here is an apparent electric conductivity, which inherently includes dielectric losses.

[26] As expected, neglecting the electric conductivity has also an effect on the estimation of the antenna elevation. For instance, in the 1000–2000 MHz frequency range, the average error performed on the inverse estimation of d_0 is 2.97×10^{-4} m and the error is 1.07×10^{-3} when deriving d_0 from t_i. Errors of about one order of magnitude larger are observed in the 100–900 MHz frequency range.

3.2.3. Model Configuration c: Source Over a Two-Layered Medium

[27] In configuration c, the source is situated above a two-layered medium (including half-space) with varying thicknesses for the top layer (d_1 = 0.005, 0.01, 0.02, 0.04, 0.08 m) and assuming the apparent electric conductivity to be frequency dependent (see Figure 2). Figure 6 represents the estimated relative dielectric permittivity using the two estimation methods. Only $\Delta d_0 = 0$ cm is considered here for the common reflection method. The top layer (layer 1) was subject to a single volumetric water content (θ = 0.158) and the lower half-space (layer 2) was subject to the nine water contents. For the case where the two layers have the same water content, i.e., the same electromagnetic properties, this model configuration reduces to configuration b, and better estimations are obtained in the 1000–2000 MHz frequency range. In general, when layer 1 is sufficiently thin (d_1 = 0.005 m), the estimated dielectric permittivity tends to the dielectric permittivity of layer 2. However, for large dielectric contrasts, absolute errors on ε_r may reach about 1 (corresponding to an error on θ of about 0.03) for the 100–900 MHz frequency range, and about 3 (corresponding to error on θ of about 0.09) for the 1000–2000 MHz frequency range. Similarly, when layer 1 is sufficiently thick (d_1 = 0.08 m), the estimated dielectric permittivity tends to the dielectric permittivity of layer 1. For intermediate layer thicknesses, either intermediate or unrealistic values are obtained. The error on the estimated dielectric permittivity increases with the dielectric contrast. Similar results are obtained for both the common reflection and inversion methods.

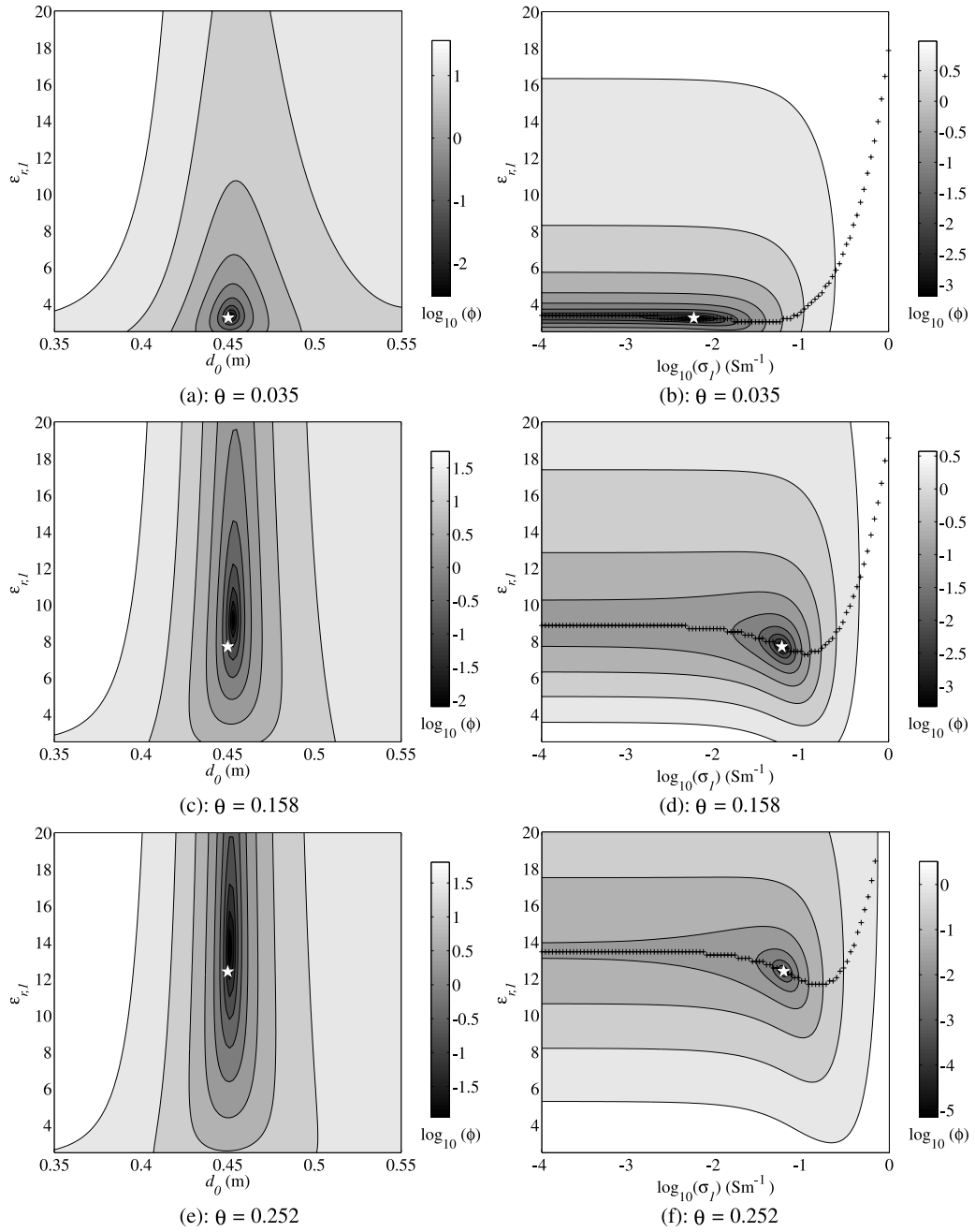

Figure 4. The 100–900 MHz response surfaces of the objective function logarithm $\log_{10}(\phi)$ in the $\varepsilon_r - h$ and $\varepsilon_r - \sigma$ parameter planes for three different volumetric water contents θ. The star represents the true parameter values. The pluses represent the minimum region of the objective function with respect to the electric conductivity σ.

[28] Figure 7 illustrates the effect of layering on the surface reflection. When there is no layering ($\theta_1 = \theta_2$), the amplitude of the reflection depends directly on the electromagnetic contrast between the air and the soil surface. However, when layering is present, the reflections at the different interfaces may interfere in a constructive or destructive way and lead to a larger or smaller reflection amplitude. In Figure 7 an example of constructive interference is given and the resulting overestimation of the dielectric permittivity can be observed in Figure 6d ($\theta_2 = 0.010$, $\varepsilon_r = 16.16$, $d_1 = 0.02$ m).

[29] The presence of these interferences depends on the ratio between the wavelength λ_1 and layer thickness d_1, and on the electromagnetic contrast between the layers. Two cases can be distinguished. First, if $d_1 < \lambda_1/2$ and the reflection coefficient at the interface between the two layers is positive, then constructive interferences will appear and they will be maximum for $d_1 = \lambda_1/4$. Second, if $d_1 < \lambda_1/2$ but the reflection coefficient is negative, then interferences will be destructive. This phenomenon is illustrated in Figure 8 representing the estimated water content as a function of the thickness d_1 of the top layer, using the common reflection method. We can observe that when the

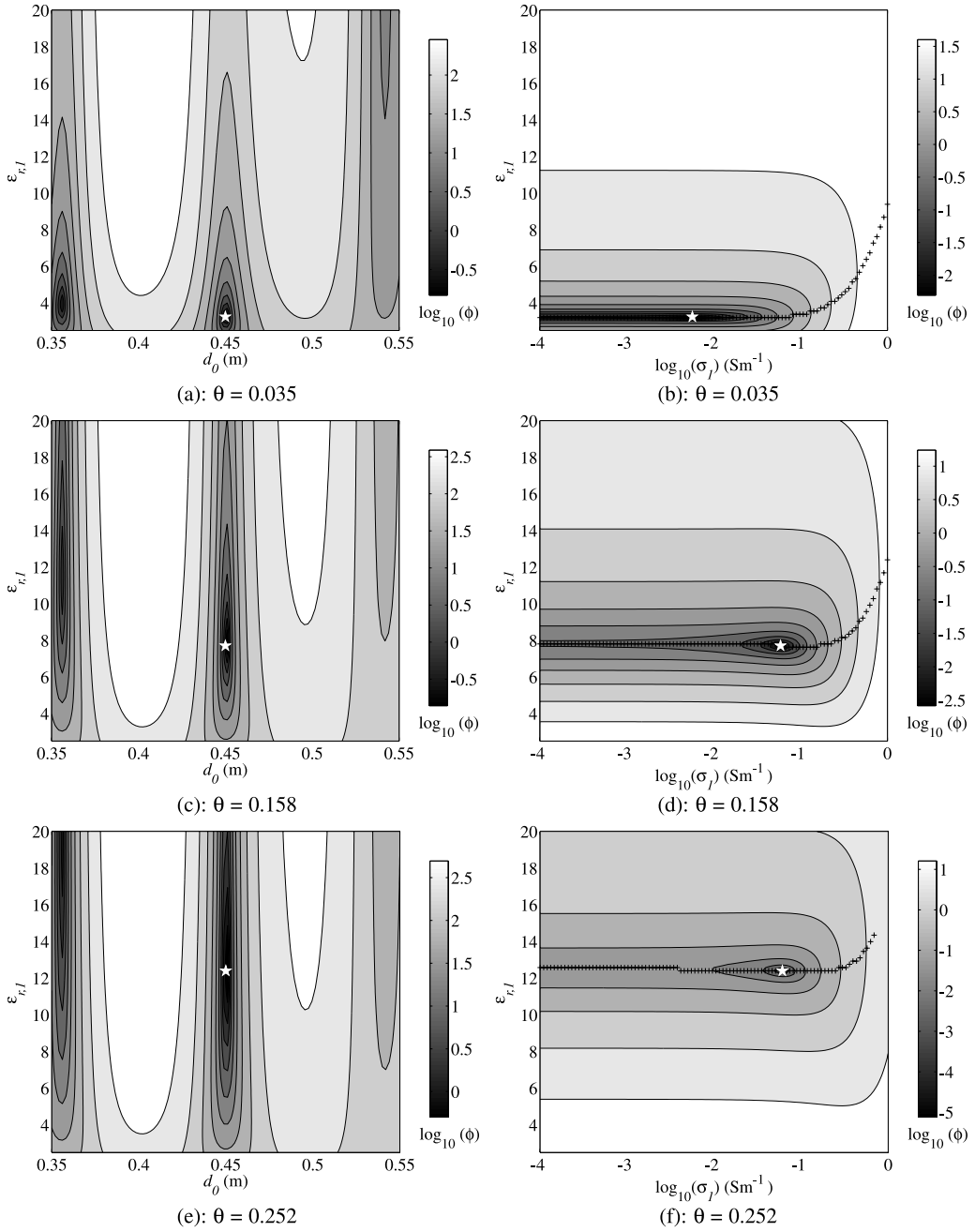

Figure 5. The 1000–2000 MHz response surfaces of the objective function logarithm $\log_{10}(\phi)$ in the $\varepsilon_r - h$ and $\varepsilon_r - \sigma$ parameter planes for different volumetric water contents θ. The star represents the true parameter values. The pluses represent the minimum region of the objective function with respect to the electric conductivity σ.

thickness of the top layer tends to zero, then the estimated water content pertains as expected to the lower half-space. When d_1 is sufficiently high, then the estimated water content tends to the water content of the surface layer. The first-order interferences are visible below $\lambda_1/2$. The remaining oscillating behavior is an artefact of the inverse Fourier transform when using data in a limited frequency window and constitutes interferences of higher orders. It is worth emphasizing here that when $d_1 = \lambda_1/4$, the error on the estimated water content may be extremely large.

[30] In the scenarios of Figure 6 the average $\lambda_1/4$ is 0.054 m for the 100–900 MHz band and 0.018 m for the 1000–2000 MHz band. These values correspond well to the layer thicknesses for which the largest discrepancies are observed. In practical applications, the presence of large electromagnetic contrasts may be favored by the direct exposure of the soil surface to the weather conditions (sun, wind, precipitation). However, due to transfer phenomena, these contrasts naturally disappear with time.

3.2.4. Model Configuration d: Three-Layered Laboratory Setup

[31] Configuration d corresponds to the laboratory experiment described below. It consists in a source situated above a three-layered medium whose lower half-space is a PEC

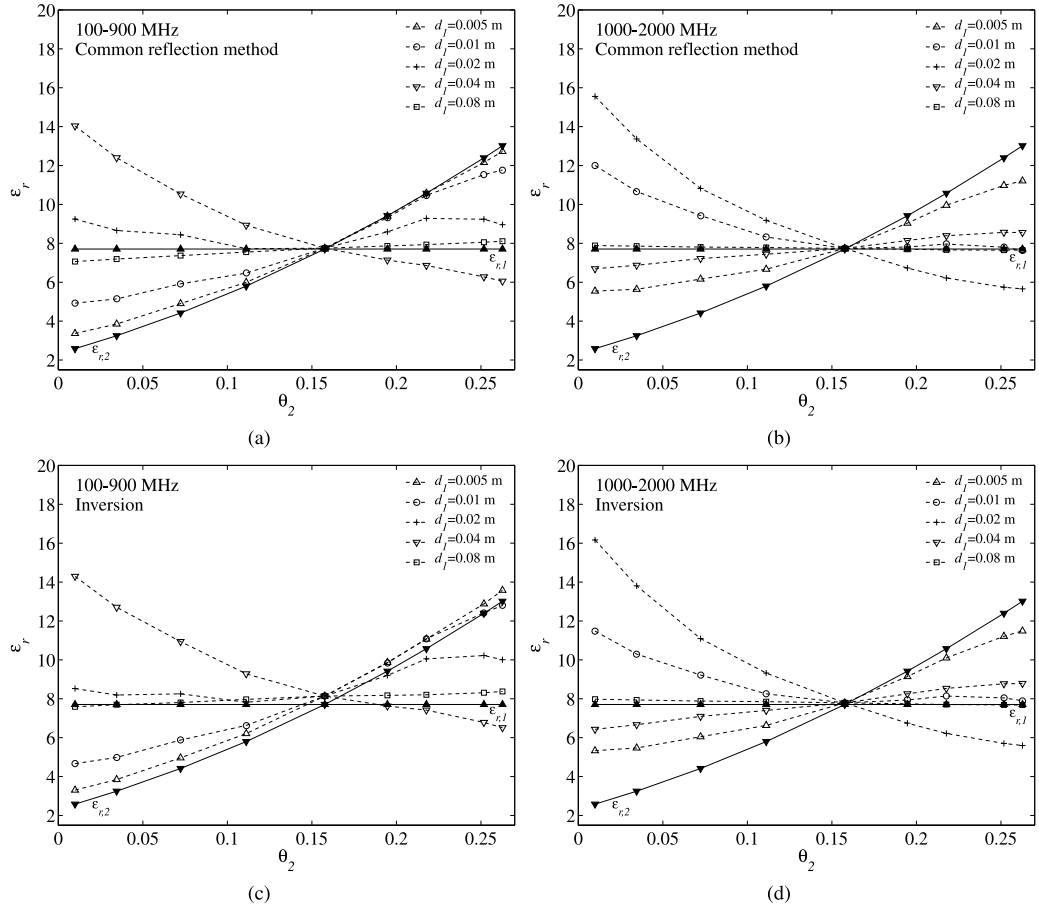

Figure 6. Relative dielectric permittivity (ε_r) as a function of the volumetric water content (θ) for model configuration c, a source over a two-layered medium, considering five different values for the thickness d_1 of the topsoil layer and two frequency ranges (100–900 and 1000–2000 MHz). The solid lines represent the true dielectric permittivity values of the soil layers. The dashed lines represent the estimated values using both the common reflection and inversion methods.

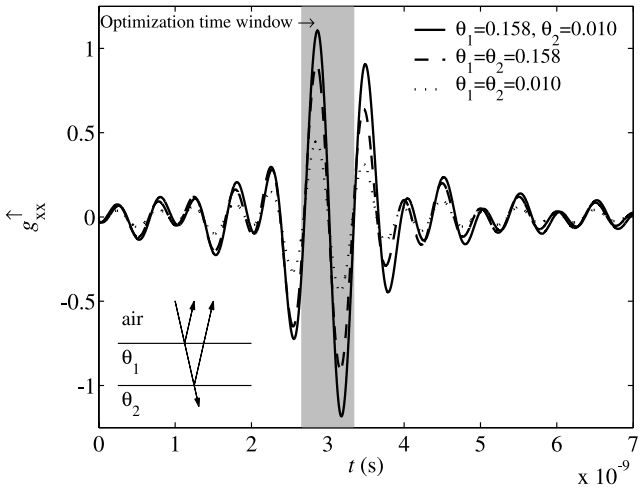

Figure 7. Synthetic Green's functions generated for configuration c, a source over a two-layered medium, with d_1 = 0.02 m and different water contents. An outline illustrates the constructive interference between the reflections originating from the two layer interfaces.

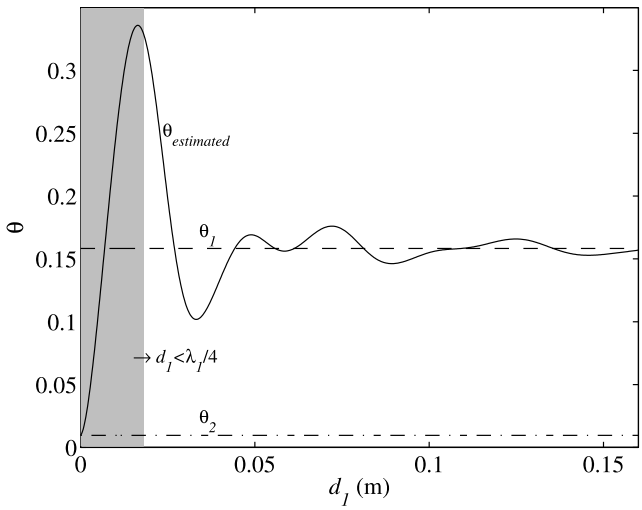

Figure 8. Estimated volumetric water content θ using the common reflection method as a function of thickness d_1 of the top layer for configuration c, a source over a two-layered medium. The water contents of layers 1 and 2 are θ_1 = 0.158 and θ_2 = 0.010, respectively. The shaded area delineates the depth resolution zone defined by one fourth the average wavelength λ in the medium.

(see Figure 2). The apparent electric conductivity is assumed to be frequency dependent. Results are presented in Table 1. Since the surface layer is relatively thick ($d_1 = 0.15$ m), layering effects are expected to be of minor importance. The full-wave inversion method appears here to outperform the common reflection method. In the frequency range 1000–2000 MHz, which corresponds to the laboratory experiment presented below, $s_{\theta 1} = 5.68 \times 10^{-3}$ for the inversion method and $s_{\theta 1} = 1.01 \times 10^{-2}$ for the common reflection method with $\Delta d_0 = 0$. These results show the theoretical limitations on the accuracy that can be achieved with these techniques in the particular case of the laboratory experiment presented below. In practical applications, measurements and modeling errors are inherently present and the presented results are expected to be reduced.

3.3. Laboratory Experiment

3.3.1. Radar System and Measurements

[32] The objective of the laboratory experiment is to investigate the stability of the inverse solution with respect to actual measurement and modeling errors in controlled conditions. The laboratory experiment is fully described by *Lambot et al.* [2004c] and the model configuration corresponds closely to configuration d in Figure 2.

[33] We used an ultrawide band SFCW radar combined with an off-ground monostatic horn antenna. The radar system was set up using a VNA (ZVRE, Rohde & and Schwarz, Munich, Germany) with an excellent dynamic range (>130 dB). The antenna system consisted of a linear polarized double-ridged broadband horn (BBHA 9120 D, Schwarzbeck Mess-Elektronik, Schönau, Germany). Antenna dimensions are 22 cm length and 14×24 cm^2 aperture area and the nominal frequency range is 1–18 GHz. The relatively small 3-dB beam width of the antenna (27° in the E plane and 22° in the H plane at 2 GHz) makes it suitable for using off ground. Measurements were performed with the antenna aperture situated at an average height of ~40 cm above the soil surface (phase center at ~47 cm).

[34] The antenna was connected to the reflection port of the VNA via a high quality N type 50 Ohm impedance coaxial cable of 2.5 m length (Sucoflex 104PEA, Huber + Suhner AG, Herisau, Switzerland). We calibrated the VNA at the connection between the antenna feed point and the cable. The frequency-dependent complex ratio $S_{11}(\omega)$ between the returned signal and the emitted signal was measured sequentially at 126 evenly stepped operating frequencies over the range 1–2 GHz using a 8 MHz frequency step.

[35] Radar measurements were carried out on a tank made of wood (1.45×1.30 m^2 area) filled with a two-layered disturbed sandy soil. The top sand layer was subject to nine different water contents (volumetric values: θ = 0.000, 0.038, 0.081, 0.119, 0.146, 0.200, 0.208, 0.256, 0.263), while the bottom layer was kept to a constant water content ($\theta = 0.100$). The thickness of the bottom layer was equal to 0.13 m, whereas the thickness of the top sand layer varied from about 0.10–0.14 m, as a function of the imposed water content level. Below the sand layer, a horizontal metal sheet (PEC) was installed to control the bottom boundary condition in the electromagnetic model.

3.3.2. Inversion Results

[36] An example of measured and modeled time domain Green's functions for three different water contents is shown in Figure 9. The position of the layers in the time domain is also illustrated. The positions in time were inferred from the known layer thicknesses and wave propagation times for the different layer permittivities. We can clearly observe the increasing propagation time in layer 1 with increasing water content. The reflections at the interface between the two sand layers and at the metal sheet decrease substantially when increasing water content in the first layer. The measured signal at the level of the surface reflection is accurately reproduced by the electromagnetic model. As the model used for the inversions consists of only a lower half-space, the reflections from the subsequent layers are naturally not reproduced by the model. The reflection at the surface is automatically detected in the time domain and serves to determine the time window in which the inversion is performed.

[37] Inversion results are presented in Table 1 and Figure 10. First, we can observe that compared to the reference frequency domain inversions assuming the correct model configuration [see *Lambot et al.*, 2004c], for which $s_{\theta 1} = 8.23 \times 10^{-3}$, estimations from the surface reflection lead to less satisfactory results ($s_{\theta 1} = 2.22 \times 10^{-2}$ for the inversion and $s_{\theta 1} = 2.81 \times 10^{-2}$ for the common reflection method). Both methods lead to similar results, with slightly better results for the inversion method.

[38] The origin of the observed discrepancies is twofold. First, the solution may be quite sensitive to actual measurement and modeling errors. However, Figure 10 shows that these errors are relatively small compared to the variation range. Second, the water content in the top sand layer was not sufficiently homogeneous and therefore the water content measured with the radar, pertaining approximately to the top 2 cm of the sand, is different from the volumetric water content determined using the reference method, pertaining approximately to the depth range 2–7 cm. For instance, *Serbin and Or* [2004] showed that surface reflection GPR measurements were in good agreement with volumetric measurements for the top 1-cm layer of soil, but did not agree well with underlying TDR and volumetric data.

4. Summary and Conclusion

[39] We show in this paper that full-wave forward modeling and inversion of the GPR signal focused on the surface reflection presents substantial advantages compared to the common surface reflection method, which is more prone to errors. First, the antenna model permits to remove the antenna effects and to reach a better accuracy in the estimation of the surface dielectric permittivity and correlated water content. This is particularly true when the antenna is situated relatively close to the ground, e.g., to achieve a better horizontal resolution. Second, the inversion method neither requires a priori knowledge of the height of the antenna above the ground nor does it require to perform corresponding measurements above a PEC. In that respect, we showed that the common surface reflection method is very sensitive to antenna height errors. For instance, a difference of 1 cm can lead to an absolute error on the water content larger than 0.02.

[40] Numerical experiments showed the physical limits of the assumptions used for estimating the surface dielectric permittivity from the surface reflection, either using the

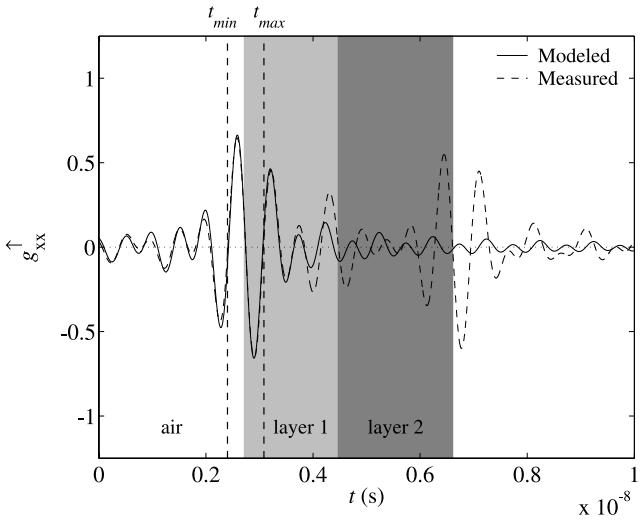

(a): θ = 0.035

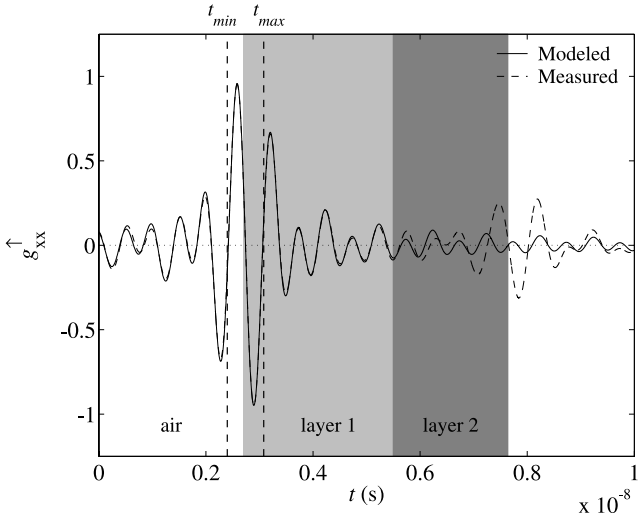

(b): θ = 0.158

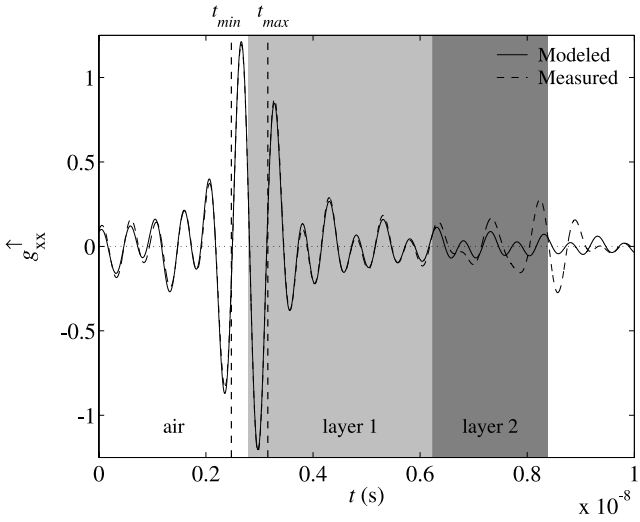

(c): θ = 0.252

Figure 9. Measured (dashed line) and modeled (solid line) Green's functions ($g_{xx}^{\uparrow}$) in the time domain for three different volumetric water contents for the laboratory experiment. The position of the layers in the time domain is represented by the shaded areas. The time window is limited by $t_{\min}$ and $t_{\max}$ (see Figure 1b).

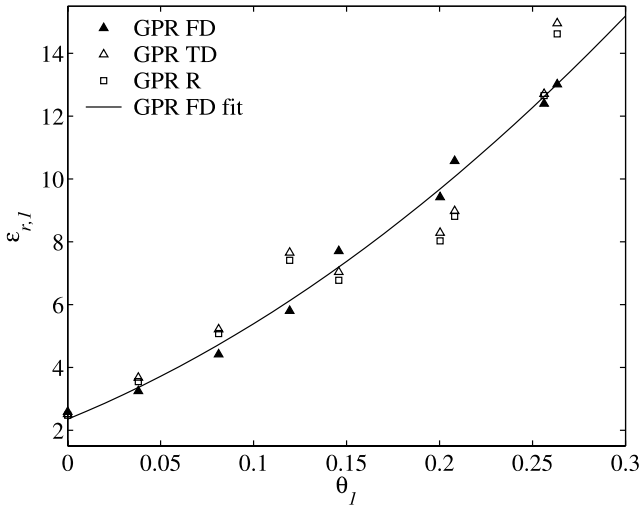

Figure 10. Relative dielectric permittivity $\varepsilon_{r,1}$ as a function of volumetric water content θ_1 for the laboratory experiment, derived from inversion in the frequency domain using the correct model configuration (GPR FD) together with the fitted relationship (GPR FD fit), from inversion focused in the time domain on the surface reflection (GPR TD), and from the common surface reflection method (GPR R).

common reflection method or full-wave inversion. In particular, the apparent electric conductivity of the soil can be neglected only if it is <0.1 Sm^{-1}, depending on the operating frequency range. If this condition is not strictly respected, unrealistic values may be obtained for the surface dielectric permittivity and volumetric water content. Moreover, the presence of contrasted layering in the topsoil may affect significantly the estimations and lead as well to unrealistic values. Ideally, the soil should be sufficiently smooth till a depth corresponding to at least one half of the average wavelength, which corresponds to the characterization scale depth.

[41] Provided that the requirements described above are respected and Rayleigh's criterion is satisfied for soil roughness, we recommend the use of the full-wave inverse modeling approach compared to the common reflection method as it is more practical and robust. It inherently leads to significantly more accurate results for the estimation of the surface water content. It is worth noting that particular attention should be given to the characterization scale and depth when comparing the radar data to ground truth measurements. Further theoretical research needs to address the possibility of taking into account layering and electric conductivity in the inversion procedure and the effect of vegetation should be investigated. Accurate knowledge of the surface dielectric permittivity and antenna height is also

very useful to further determine the underlying soil properties, e.g., in the root zone, from the radar data.

[42] **Acknowledgments.** This research was supported by a Marie Curie IntraEuropean Fellowship within the 6th European Community Framework Programme, Delft University of Technology (Netherlands), the Université catholique de Louvain (Belgium), and the Forschungszentrum Jülich GmbH (Germany). We thank two anonymous reviewers for their constructive comments.

References

al Hagrey, S. A., and C. Müller (2000), GPR study of pore water content and salinity in sand, *Geophys. Prospect.*, *48*, 63–85.

Annan, A. P. (2002), GPR—History, trends, and future developments, *Subsurface Sensing Technologies and Applications*, *3*, 253–270.

Boithias, L. (1987), *Radio Wave Propagation*, McGraw-Hill, New York.

Chanzy, A., A. Tarussov, A. Judge, and F. Bonn (1996), Soil water content determination using digital ground penetrating radar, *Soil Sci. Soc. Am. J.*, *60*, 1318–1326.

Davis, J. L., and A. P. Annan (2002), Ground penetrating radar to measure soil water content, in *Methods of Soil Analysis*, part 4, *Physical Methods*, edited by J. Dane and G. Topp, pp. 446–463, Soil Sci. Soc. of Am., Madison, Wis.

Dobson, M. C., and F. T. Ulaby (1986), Active microwave soil moisture research, *IEEE Trans. Geosci. Remote Sens.*, *24*, 23–36.

Du, S., and P. Rummel (1994), Reconnaissance studies of moisture in the subsurface with GPR, in *Proceedings of the Fifth International Conference on Ground Penetrating Radar*, edited by M. T. van Genuchten, F. J. Leij, and L. Wu, pp. 1241–1248, Waterloo Cent. for Groundwater Res., Univ. of Waterloo, Waterloo, Ont., Canada.

Famiglietti, J. S., J. A. Devereaux, C. A. Laymon, T. Tsegaye, P. R. Houser, T. J. Jackson, S. T. Graham, M. Rodell, and P. J. van Oevelen (1999), Ground-based investigation of soil moisture variability within remote sensing footprints during the Southern Great Plains 1997 (SGP97) Hydrology Experiment, *Water Resour. Res.*, *35*, 1839–1851.

Galagedara, L. W., G. W. Parkin, and J. D. Redman (2003), An analysis of the GPR direct ground wave method for soil water content measurement, *Hydrol. Processes*, *17*, 3615–3628.

Galagedara, L. W., G. W. Parkin, J. D. Redman, P. von Bertoldi, and A. L. Endres (2005a), Field studies of the GPR ground wave method for estimating soil water content during irrigation and drainage, *J. Hydrol.*, *301*, 182–197.

Galagedara, L. W., J. D. Redman, G. W. Parkin, A. P. Annan, and A. L. Endres (2005b), Numerical modeling of GPR to determine the direct ground wave sampling depth, *Vadose Zone J.*, *4*, 1096–1106.

Grote, K., S. S. Hubbard, and Y. Rubin (2003), Field-scale estimation of volumetric water content using GPR ground wave techniques, *Water Resour. Res.*, *39*(11), 1321, doi:10.1029/2003WR002045.

Huisman, J. A., C. Sperl, W. Bouten, and J. M. Verstraten (2001), Soil water content measurements at different scales: Accuracy of time domain reflectometry and ground penetrating radar, *J. Hydrol.*, *245*, 48–58.

Huisman, J. A., J. J. J. C. Snepvangers, W. Bouten, and G. B. M. Heuvelink (2002), Mapping spatial variation in surface soil water content: Comparison of ground-penetrating radar and time domain reflectometry, *J. Hydrol.*, *269*, 194–207.

Huisman, J. A., S. S. Hubbard, J. D. Redman, and A. P. Annan (2003), Measuring soil water content with ground penetrating radar: A review, *Vadose Zone J.*, *2*, 476–491.

Jackson, T.-J., J. Schmugge, and E.-T. Engman (1996), Remote sensing applications to hydrology: Soil moisture, *Hydrol. Sci.*, *41*, 517–530.

Lagarias, J. C., J. A. Reeds, M. H. Wright, and P. E. Wright (1998), Convergence properties of the Nelder-Mead simplex method in low dimensions, *SIAM J. Optim.*, *9*, 112–147.

Lambot, S., M. Antoine, I. van den Bosch, E. C. Slob, and M. Vanclooster (2004a), Electromagnetic inversion of GPR signals and subsequent hydrodynamic inversion to estimate effective vadose zone hydraulic properties, *Vadose Zone J.*, *3*, 1072–1081.

Lambot, S., J. Rhebergen, I. van den Bosch, E. C. Slob, and M. Vanclooster (2004b), Measuring the soil water content profile of a sandy soil with an off-ground monostatic ground penetrating radar, *Vadose Zone J.*, *3*, 1063–1071.

Lambot, S., E. C. Slob, I. van den Bosch, B. Stockbroeckx, and M. Vanclooster (2004c), Modeling of ground-penetrating radar for accurate characterization of subsurface electric properties, *IEEE Trans. Geosci. Remote Sens.*, *42*, 2555–2568.

Lambot, S., I. van den Bosch, B. Stockbroeckx, P. Druyts, M. Vanclooster, and E. C. Slob (2005a), Frequency dependence of the soil electromagnetic properties derived from ground-penetrating radar signal inversion, *Subsurface Sens. Technol. Appl.*, *6*, 73–87.

Lambot, S., L. Weihermüller, I. van den Bosch, M. Vanclooster, and E. C. Slob (2005b), Full-wave inversion of off-ground monostatic GPR signal focused on the surface reflection for identifying surface dielectric permittivity, in *Proceedings of the 3rd International Workshop on Advanced Ground Penetrating Radar*, edited by S. Lambot and A. Gorriti, pp. 113–118, Delft Univ. of Technology, Delft, Netherlands.

Lambot, S., M. Antoine, M. Vanclooster, and E. C. Slob (2006), Effect of soil roughness on the inversion of off-ground monostatic GPR signal for noninvasive quantification of soil properties, *Water Resour. Res.*, *42*, W03403, doi:10.1029/2005WR004416.

Ledieu, J., P. D. Ridder, P. D. Clercq, and S. Dautrebande (1986), A method of measuring soil moisture by time domain reflectometry, *J. Hydrol.*, *88*, 319–328.

Merz, B., and A. Bardossy (1998), Effect of spatial variability on the rainfall runoff process in a small loess catchment, *J. Hydrol.*, *212*, 304–317.

Michalski, K. A., and J. R. Mosig (1997), Multilayered media Green's functions in integral equation formulations, *IEEE Trans. Antennas Propag.*, *45*, 508–519.

Redman, J. D., J. L. Davis, L. W. Galagedara, and G. W. Parkin (2002), Field studies of GPR air launched surface reflectivity measurements of soil water content, *Proc. SPIE Int. Soc. Opt. Eng.*, *4758*, 156–161.

Serbin, G., and D. Or (2003), Near-surface water content measurements using horn antenna radar: Methodology and overview, *Vadose Zone J.*, *2*, 500–510.

Serbin, G., and D. Or (2004), Ground-penetrating radar measurement of soil water content dynamics using a suspended horn antenna, *IEEE Trans. Geosci. Remote Sens.*, *42*, 1695–1705.

Serbin, G., and D. Or (2005), Ground-penetrating radar measurement of crop and surface water content dynamics, *Remote Sens. Environ.*, *96*, 119–134.

Ulaby, F., M. Moore, and A. Fung (1986), *Microwave Remote Sensing: Active and Passive*, vol. III, *From Theory to Applications*, Artech House, Norwood, Mass.

Warnick, K. F., and W. C. Chew (2001), Numerical simulation methods for rough surface scattering, *Waves Random Media*, *11*, R1–R30.

Yelf, R. (2004), Where is true time-zero?, in *Proceedings of the Tenth International Conference on Ground Penetrating Radar*, edited by E. Slob, A. Yarovoy, and J. Rhebergen, pp. 279–282, Delft Univ. of Technol., Delft, Netherlands.

J. A. Huisman, S. Lambot, H. Vereecken, and L. Weihermüller, Agrosphere (ICG IV), Institute of Chemistry and Dynamics of the Geosphere, Forschungszentrum Jülich GmbH, D-52425 Jülich, Germany. (s.lambot@fz-juelich.de)

E. C. Slob, Department of Geotechnology, Delft University of Technology, Mijnbouwstraat 120, N-2628 RX Delft, Netherlands.

M. Vanclooster, Department of Environmental Sciences and Land Use Planning, Université catholique de Louvain, Croix du Sud 2 Box 2, B-1348 Louvain-la-Neuve, Belgium.